doi:10.26443/seismica.v4i1.1425

Detecting seasonal differences in high-frequency site response using κ_0

Annabel Haendel * [1], **Marco Pilz** [1], **Luca C. Malatesta** [1], **David Litwin** [1], **Fabrice Cotton** [1,2]

[1]GFZ Helmholtz Centre for Geosciences, Potsdam, Germany, [2]Institute of Geosciences, University of Potsdam, Potsdam, Germany

Author contributions: *Conceptualization*: Annabel Haendel, Marco Pilz, Fabrice Cotton. *Formal Analysis*: Annabel Haendel. *Writing - Original draft*: Annabel Haendel. *Writing - Review & Editing*: Annabel Haendel, Marco Pilz, Luca Malatesta, David Litwin, Fabrice Cotton.

Abstract Near-surface geologic site conditions significantly affect seismic waves by amplifying certain frequency ranges and attenuating others. For seismic hazard analysis, site conditions are assumed to be constant over time. Contrary to this assumption, temporal variations in near-surface velocities have been observed in recent years. This study shows for the first time that $\Delta\kappa_0$, the site component of the spectral decay parameter κ derived between a surface and a borehole sensor, can vary seasonally. $\Delta\kappa_0$ is an integrative parameter of local site attenuation and amplification at high frequencies. Using data from the Kiban Kyoshin Strong Motion Network (KiK-net) in Japan, we analyze recordings of seismic events between 2004–2020 and correlate temporal $\Delta\kappa_0$ variations with environmental factors such as temperature, precipitation, snow depth, soil moisture, and terrestrial water storage. We can identify strong seasonal variations at 13 sites in northeastern Hokkaido and on Honshu, with $\Delta\kappa_0$ being generally larger in winter than in summer. Our results indicate that the high-frequency site response can be influenced by environmental conditions and should not be assumed to be constant.

Production Editor: Théa Ragon
Handling Editor: Vitor Silva
Copy & Layout Editor: Anna Ledeczi

Received: 7 August 2024
Accepted: 21 May 2025
Published: 11 June 2025

1 Introduction

Near-surface geologic site conditions can strongly modify seismic waves as they travel to the surface. For example, certain frequency ranges will be amplified if there is a strong impedance contrast in the ground. On the other hand, physical processes such as material damping or scattering attenuate the incoming wavefield, resulting in a low-pass filtering effect. Each site therefore has a specific site response that depends on the particular subsoil conditions and 3D surface and subsurface structure.

Near-surface materials are sensitive to environmental perturbations. For example, near-surface seismic wave velocities are sensitive to atmospheric temperature fluctuations (Richter et al., 2014; Hillers et al., 2015), precipitation (e.g. Hillers et al., 2014; Wang et al., 2017; Miao et al., 2018), soil moisture in the uppermost 10 m (Shen, 2022), groundwater level (e.g. Sens-Schönfelder and Wegler, 2006; Illien et al., 2021; Mao et al., 2022), the freezing of the ground in winter (Miao et al., 2019) or the thawing of the active permafrost layer in summer (e.g. James et al., 2019). As a consequence of seismic velocity changes, the overall site response also changes, as measured for example by the horizontal-to-vertical spectral ratio (HVSR, Nakamura, 1989). Vassallo et al. (2022) studied 12 years of continuous seismic data in central Italy and report an increase in the HVSR peak frequency during spring and summer due to a velocity increase, and a decrease in the HVSR peak frequency during winter. Temporal variations of the HVSR have also been used to monitor the temporal variability of the active permafrost layer (Kula et al., 2018; Köhler and Weidle, 2019), which acts as a strong impedance contrast in summer at 1–2 m depth and leads to resonance and increased shaking between 35–45 Hz. Colombero et al. (2018) and Lotti et al. (2018) found that the observed HVSR changes at unstable rock flank sites are controlled by daily and seasonal variations in air temperature. Li and Ben-Zion (2023) observe daily and seasonal changes in seismic velocities at 50 seismic stations in southern California by combining HVSR with the autocorrelation method.

The influence of environmental variations on seismic attenuation, which affects the amplitude of the shaking, is less well understood but has also been observed. For example, Malagnini et al. (2019) report that seismic attenuation derived from repeated earthquakes at Parkfield appears to be sensitive to seasonal hydrological loading and polar tides. Another common parameter used to describe local site attenuation is κ_0, the path-independent component of κ (Anderson and Hough, 1984). κ is measured as the amplitude decay of the Fourier acceleration spectrum at high frequencies. κ_0 is then obtained by extrapolating the values of κ obtained from earthquakes at different distances to zero distance. κ_0 can be attributed to local site attenuation (Anderson and Hough, 1984), but also to possible source effects (e.g. Papageorgiou and Aki, 1983; Beresnev, 2019) or to attenuation near the fault (Kilb et al., 2012; Bindi et al., 2019). If a surface and a borehole station are available at the same site, the site effect term due to layers between the surface and borehole can be clearly separated from

*Corresponding author: ahaendel@gfz.de

possible source terms by calculating $\Delta\kappa_0$ between the two stations.

The value of κ_0 can be very different from site to site, depending on the local geology. However, the value of κ, and hence κ_0, at a site also depends on the database and pre-processing choices (Ktenidou et al., 2013; Ji et al., 2020), the selected frequency window of the estimation (Edwards et al., 2015; Mayor et al., 2018; Haendel et al., 2020; Tafreshi et al., 2022), the earthquake type and focal depth of the selected events (Ji et al., 2020), the installation and housing of the sensor (Hollender et al., 2020) and the nonlinear soil behavior induced by strong ground motions (Van Houtte et al., 2014; Ji et al., 2021; Xu and Rathje, 2021). These factors contribute to the within-station variability of κ_0 (the scatter in κ_0 at a single site) which has been found to be high and can sometimes be comparable to or even exceed the site-to-site variability of κ_0 (Bora et al., 2017; Ji et al., 2020; Tafreshi et al., 2022). Typically, a single site term κ_0 is calculated for each station, and it is assumed that this term is constant over time. We will show that this assumption is not necessarily true and that temporal variations of κ_0 can contribute to the observed within-station variability.

In this study, we want to investigate whether $\Delta\kappa_0$ recorded between a borehole and the surface varies with time, similar to near-surface wave velocity and HVSR. Because of the dense station coverage and the availability of surface-borehole station pairs, we focus the $\Delta\kappa_0$ analysis on data from the Kiban Kyoshin Strong Motion Network (KiK-net) in Japan (Aoi et al., 2004, see also 'Data and code availability' section). As we will show later, $\Delta\kappa_0$ is an integrated parameter that is sensitive to both attenuation and subsurface amplification at high frequencies, and is therefore a sensitive tool for identifying temporal variations in the very shallow subsurface. We will correlate temporal $\Delta\kappa_0$ curves with various environmental parameters such as temperature and precipitation, but also with parameters derived from satellite measurements such as soil moisture and terrestrial water storage. Finally, we will examine potential drivers of $\Delta\kappa_0$ changes, providing preliminary insights, and we will place our findings in the context of other studies conducted in Japan.

2 Method

The parameter κ describes the amplitude decay of the Fourier acceleration spectrum at high frequencies using an exponential form (Anderson and Hough, 1984)

$$a(f) = a_0 \exp\{[-\pi f \kappa]\} \qquad f > f_e, \tag{1}$$

where a_0 combines the frequency independent contributions from the source and the site, while f_e is the frequency above which the spectrum decays. The path-independent term κ_0 can be derived by plotting κ as a function of epicentral distance R_{epi}

$$\kappa = \kappa_0 + R_{epi} \cdot \kappa_R. \tag{2}$$

The term κ_R describes the attenuation along the traveling path of the wave. The zero-distance intercept κ_0 is a constant and does not change with time if Eq. 2 is applied for all recordings of a site.

In this publication we work with $\Delta\kappa_{0,i}$ between a borehole-surface station pair. $\Delta\kappa_{0,i}$ is computed for all i recordings at a site using

$$\Delta\kappa_{0,i} = \kappa_{i,\text{surface}} - \kappa_{i,\text{borehole}}. \tag{3}$$

$\Delta\kappa_{0,i}$ is insensitive to path effects but also to possible variations of the seismic source, so that we can investigate the contributions of κ_0 between the surface and borehole sensors as a function of time. As we will show in the discussion, we do not treat $\Delta\kappa_0$ as a pure attenuation parameter due to site effects in the measurement band of many sites. Rather, we see it as a tool to identify temporal variations in the high frequency site response, because a slope (which κ_0 is) is very sensitive to detecting temporal changes.

3 Data selection and processing

The basis for this study is the dataset used in Haendel et al. (2023), where κ_0 was calculated for 175 KiK-net locations throughout Japan. Typical borehole depth is 100–200 m, but few boreholes are as deep as 1000 m. We added some additional sites, so that a total of 188 sites where examined in this study (Fig. 1, see Table S1 in the electronic supplement).

For the data selection, we use only recordings from events with a magnitude Mw>3.5 that occurred within an epicentral distance of less than 150 km. To increase the number of recordings for better temporal resolution, and because we are focusing solely on $\Delta\kappa_0$, we included all earthquakes with a focal depth less than 150 km (as opposed to the 50 km limit used in Haendel et al. (2023)). We excluded events with a peak ground acceleration (PGA) of 0.5 m/s^2 or higher at the surface to avoid strong nonlinear effects in our time series. The remainder of the data processing follows the procedure described in Haendel et al. (2023), of which we summarize the main steps in the following.

κ is calculated from the S-wave window of a recording. The start of the S-wave window is derived using the TauPy toolkit implemented in ObsPy (Beyreuther et al., 2010) and the length of the S-wave window D_S is computed following the definition for the S-wave window duration in Perron et al. (2018). The extracted S-wave window is then demeaned, tapered at the edges with a 5% cosine taper and padded with zeros before the Fourier transform is performed. The Fourier amplitude spectrum is smoothed with a Hanning window of 2 Hz length. To obtain a single and azimuthally independent spectrum, we compute the root-mean square (RMS) of the two horizontal components in the form $\text{RMS} = \sqrt{\frac{1}{2}(\text{NS}^2 + \text{EW}^2)}$, where NS and EW are the north-south and east-west components respectively. We choose a fixed frequency band of 12–24 Hz for κ measurements (Eq. 1) to make κ comparable between different recordings. The lower limit of 12 Hz is chosen to avoid the influence of the source corner frequency. The upper limit of 24 Hz is just below the frequency (25 Hz) at which the instrument response of the KiK-net stations

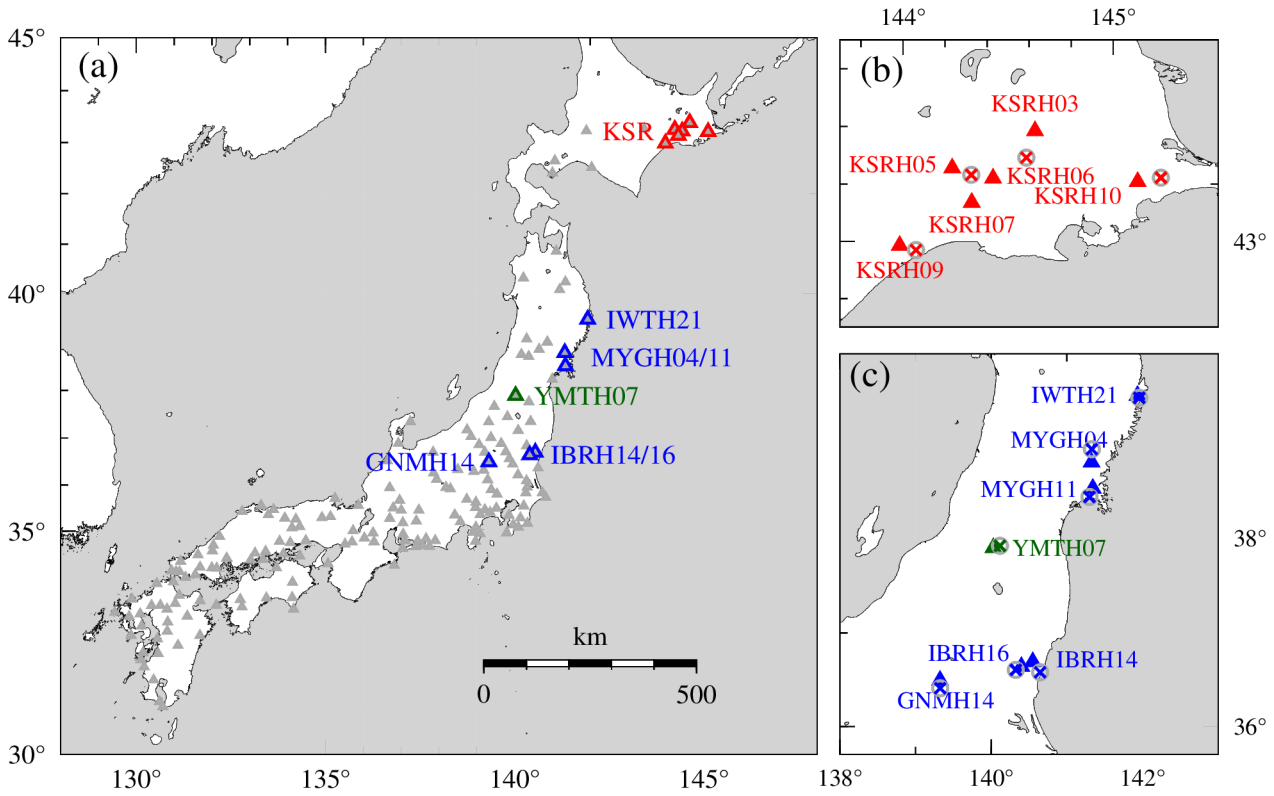

Figure 1 (a) Location of the 188 KiK-net sites analyzed in this study (gray triangles) and the 13 sites with pronounced seasonal variation in $\Delta\kappa_0$ (highlighted triangles). The different colors indicate clusters of sites that respond differently to environmental change. (b) Zoom on the northeast corner of Hokkaido and (c) Honshu. The crosses indicate the locations of JMA weather stations.

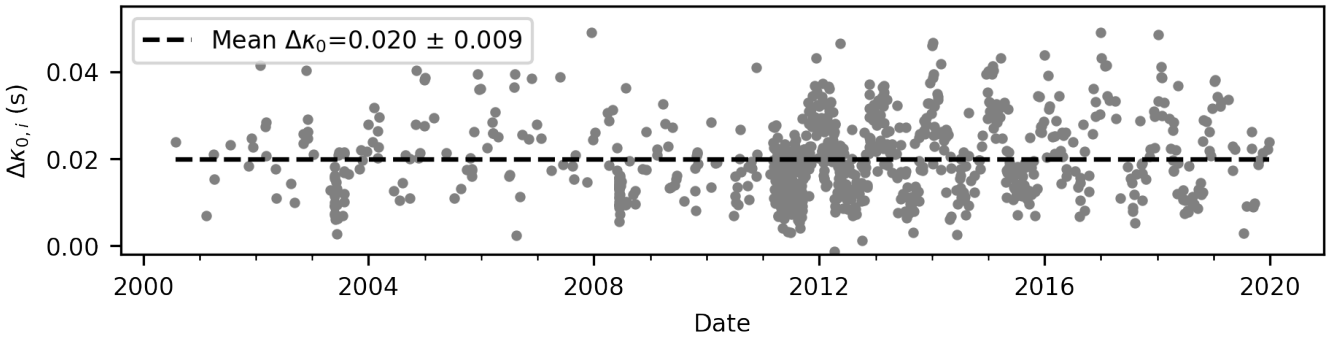

Figure 2 $\Delta\kappa_{0,i}$ as a function of time at the site IWTH21, showing seasonal variations that are evident in the 2011–2020 period.

begins to significantly affect the spectrum (Aoi et al., 2004). If the signal-to-noise ratio below 24 Hz is less than 3, a lower upper frequency limit is selected. However, the upper frequency limit must be above 22 Hz to ensure that the frequency band for κ estimation is at least 10 Hz wide. $\Delta\kappa_{0,i}$ is then derived for each surface-borehole station pair using Eq. 3.

In addition to the KiK-net data, we downloaded environmental parameters for Japan. The Japan Meteorological Agency (JMA) operates a nationwide meteorological network with more than 1400 weather stations. We downloaded daily air temperature, precipitation and snow depth values from the weather stations that are closest to the selected sites (Fig. 1). The maximum distance between a selected KiK-net site and a weather station is 15 km, but often 10 km or less. We also downloaded daily satellite soil moisture data from the Copernicus Climate Change Service (C3S) with a resolution of 0.25° (Dorigo et al., 2019). We use data from active (backscatter) microwave remote sensing

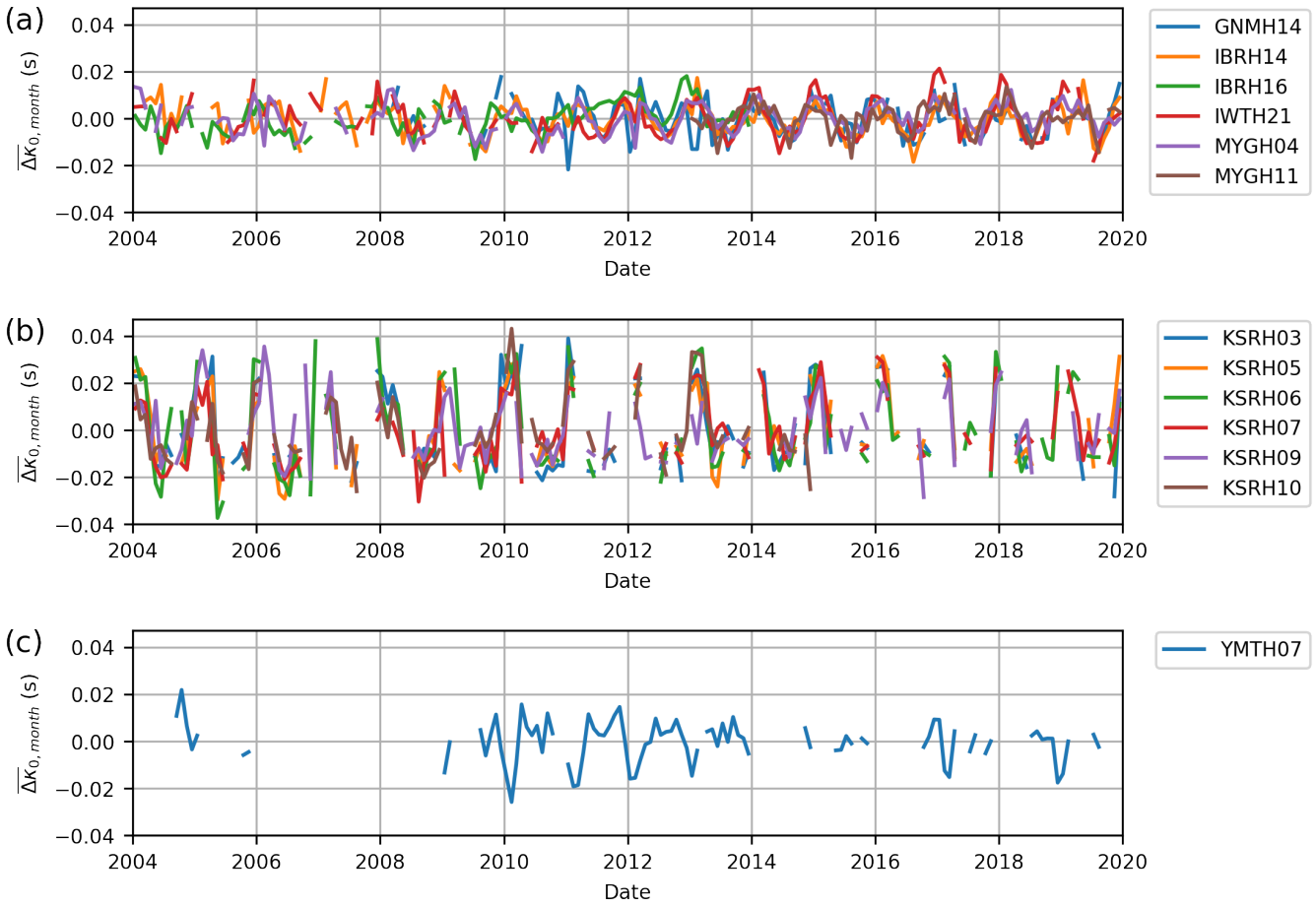

Figure 3 Monthly means of $\Delta\kappa_0$ ($\overline{\Delta\kappa}_{0,month}$) measured at (a) different sites on Honshu (blue triangles in Fig. 1), (b) sites on Hokkaido (red triangles in Fig. 1) and (c) at station YMTH07 (green triangle in Fig. 1). The overall mean $\Delta\kappa_0$ at each site (given in Table S2 in the electronic supplement) was subtracted from each $\Delta\kappa_0$ value to make the curves comparable between sites.

systems that are expressed in percentage of saturation (%). The depth range of soil moisture measurements is not deeper than 10 cm. Finally, we extracted monthly terrestrial water storage (TWS) variability from the Gravity Recovery and Climate Experiment (GRACE) and its successor the GRACE Follow-On (GRACE-FO) satellite missions. The selected TWS Level-3 products (Boergens et al., 2020) represent water mass anomalies relative to the long-term average from 2002-2020 and are the summed effect of surface water, soil moisture, deep groundwater, snow and ice. TWS data are provided at 1° spatial resolution (≈ 111 km), but the sensitivity of measuring 1–2 cm in water height changes can only be provided at a spatial scale of 300x300 km^2 or more. Therefore, we choose to work with the mean TWS of 3x3 grid cells (3°x3°) around the point of interest for a better sensitivity. The URL's for all download sites are listed in the 'Data and code availability' section.

4 Seasonal variations of $\Delta\kappa_0$

In this section, we present the results of 13 selected KiK-net sites (Fig. 1, see Table S2 in the electronic supplement). The sites are mainly located in the northeastern part of Hokkaido (KSR sites) and on the main island of Honshu. An example site with strong seasonal variations is IWTH21 shown in Fig. 2. For the time period 2011–2018, the seasonal variations of $\Delta\kappa_0$ are clearly visible with $\Delta\kappa_0 = 0.013\,\text{s} \pm 0.004\,\text{s}$ in June and $\Delta\kappa_0 = 0.030\,\text{s} \pm 0.007\,\text{s}$ in December. The seasonal trend is more difficult to discern in the period 2002–2011 because there are fewer recorded events and could be confused with a high within-station variability of unknown cause.

The observation of temporal variations is therefore associated with the condition that enough earthquake records are available at a site, and that these records are not just clustered after a single mainshock, but are well distributed over time. If these conditions are not met, temporal changes may be difficult to detect or may not be detected at all. This is the case, for example, for the island of Kyushu, where earthquake records are often too clustered to detect periodic patterns. The situation is better in northern Japan due to the Tohoku earthquake in 2011 which generated many aftershocks and increased the seismicity for several years (see also Fig. 2). The 13 selected sites shown in Fig. 1 are therefore not exhaustive, but are the sites (out of the total of 188 investigated sites) where we detect clear seasonal variations. All other sites either do not show seasonal variations or we are not able to detect them due to limited (17 sites) or clustered earthquakes (10 sites) or maybe due to the selected frequency band. Nearly

all of the 13 sites with seasonal variations of $\Delta\kappa_0$ are located in, or at the edge of, modern floodplains and wetlands. Stations GNMH14 and IBRH14 are located in small mountain valleys with a narrow floor, less than 10 m above the nearby stream. Station YMTH07 is on a fluvial terrace 40 m above the floor of a larger mountain valley.

Fig. 3 shows the monthly means of $\Delta\kappa_0$ as a function of time for two different clusters of sites and a single site YMTH07. The total mean of $\Delta\kappa_0$ at each site (reported in Table S2 in the electronic supplement) has been removed from the time series in order to make the curves comparable between different sites. There are gaps in the data for some sites, and we also omitted some time periods, e.g., due to sensor changes. The KiK network undergoes regular updates, including the installation of new sensors. At some sites, these upgrades coincide with changes in the values of $\Delta\kappa_0$, as reported by Haendel et al. (2022), but at most of the sites not. For this reason, we have not excluded these stations from our dataset. Instead, we ensured that the analyzed time periods are free of any abrupt changes in the $\Delta\kappa_0$ time series. The selected time periods for each site are given in Table S2 in the electronic supplementary material.

The first cluster consists of six sites on the main island of Honshu (Fig. 3a, blue triangles in Fig. 1). There is a difference in $\Delta\kappa_0$ of about 20 ms between summer and winter, with consistently smaller values of $\Delta\kappa_0$ in summer and larger values in winter. The strongest seasonal pattern of $\Delta\kappa_0$ can be observed at sites in the northeastern corner of Hokkaido (Fig. 3b, red triangles in Fig. 1), with smaller values of $\Delta\kappa_0$ in summer and larger values in winter. On average, the difference in $\Delta\kappa_0$ between summer and winter is about 50 ms. The seasonal pattern observed at site YMTH07 on the main island of Honshu (Fig. 3c, green triangle in Fig. 1) is opposite to the behavior observed at all the other sites. $\Delta\kappa_0$ is larger in summer and smaller in winter with a difference in $\Delta\kappa_0$ of about 20–30 ms.

In Figures 4-6 we compare $\Delta\kappa_0$ of the three clusters with monthly mean temperature, total precipitation, soil moisture and terrestrial water storage (TWS). We compute a mean curve of $\Delta\kappa_0$ from all sites of a cluster and also average the environmental parameters extracted for each site. We then compute the Pearson correlation coefficient (CC) between $\Delta\kappa_0$ and the four environmental parameters, where values of +1 (-1) would indicate perfect linear correlation (anti-correlation) and 0 would correspond to no linear correlation. Some of the y-axes in Figures 4-6 are inverted to facilitate visual comparison. The correlation coefficient at the top of each panel indicates whether the data are positively or negatively correlated. In general, the correlation is highest with mean air temperature (CC=-0.82 for Honshu sites and CC=-0.75 for Hokkaido sites), with the sole exception of station YMTH07, which has the highest correlation with soil moisture (CC=0.81). The correlation with TWS is also good (CC=0.60 for Honshu, CC=0.62 for Hokkaido and CC=-0.52 for YMTH07). However, when interpreting the correlation coefficients we have to keep in mind that TWS data are averaged over a 300x300 km^2 region using satellite data, while temperature data are obtained from nearby ground weather stations. In addition, the TWS data contain the imprint of the 2011 Mw 9.1 Tohoku earthquake. Large earthquakes lead to mass redistributions in the Earth and therefore to changes and anomalies in the gravity measurements of the GRACE satellite data (visible as a drop in the TWS and a slow recovery after March 2011). For example, using only the 2004–2011 period of the Hokkaido sites increases the correlation coefficient from 0.62 to 0.67. The weakest (but still not bad) correlation is observed with soil moisture and precipitation for the majority of sites. Note that the monthly averages of soil moisture for the Hokkaido cluster in 5(b) are based on only a few data points because soil moisture is difficult to obtain when the ground is frozen or covered with snow.

5 Discussion

5.1 Influence of site amplification on $\Delta\kappa_0$

Treating $\Delta\kappa_0$ as a measure of site attenuation is only valid if the site amplification spectrum is flat in the frequency range where $\Delta\kappa_0$ is calculated. In Figure 7 we show the surface-to-borehole spectral ratio (SBSR) for each of the sites derived using only recordings from summer or winter. The cluster of sites on Honshu has clear site amplifications within the $\Delta\kappa_0$ measurement band. For example, site IBRH14 has an SBSR amplitude 24.3 at a frequency of 14.6 Hz (Figure 7). Many of the Hokkaido sites have a more or less flat SBSR at high frequencies in summer but the site amplification becomes broader and non-flat in winter. Only site YMTH07 seems to be free of site amplification between 12-24 Hz in summer and in winter. We therefore treat $\Delta\kappa_0$ in this study not as a pure attenuation parameter, but as a parameter describing the high-frequency behavior of the Fourier spectrum, which can include both, site attenuation and amplification, and which is very sensitive to detecting near-surface changes. As a result, $\Delta\kappa_0$ can also take on negative values, as observed, for example, at site KSRH09 (Table S2).

5.2 Honshu site cluster: Correlation with water volume in the ground

The variations of $\Delta\kappa_0$ recorded at the Honshu sites correlate well with several environmental parameters as shown in Fig. 4 with the highest correlation for temperature (CC=-0.82) and the lowest for precipitation (CC=-0.43). In the following, we will have a look at these parameters separately, as correlation does not necessarily imply causality.

Richter et al. (2014) and Hillers et al. (2015) reported that thermoelastic strain induced by atmospheric temperature variations can cause seasonal seismic velocity variations. We want to test whether this hypothesis could also explain the good correlation between $\Delta\kappa_0$ and temperature on Honshu. To do so, we stack all $\Delta\kappa_0$ values observed in the period 2004–2020 at all sites of the cluster into one year and compute a smoothed curve using a Gaussian filter with a width of 6 days (Fig. 8). Despite a local minimum in January/February, $\Delta\kappa_0$ is

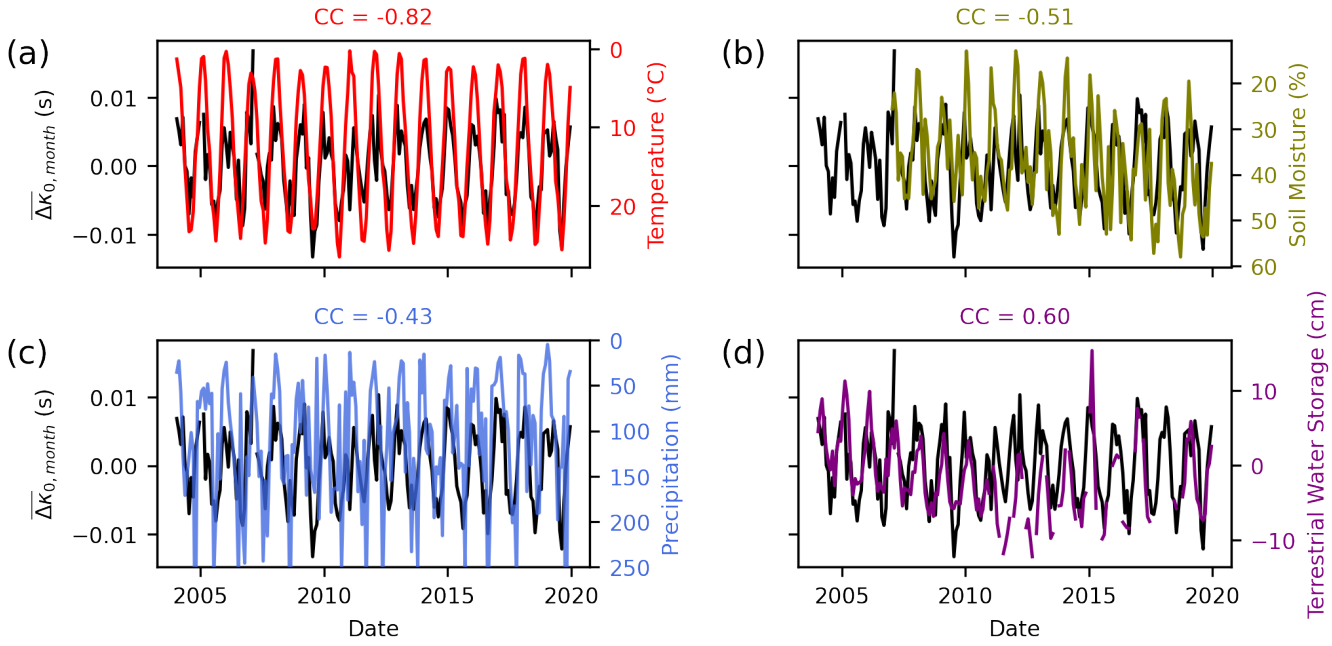

Figure 4 Monthly mean curve of $\Delta\kappa_0$ computed from all sites of the Honshu cluster (blue triangles in Fig. 1). Comparison with (a) monthly mean air temperature, (b) monthly soil moisture, (c) monthly total precipitation, and (d) terrestrial water storage (TWS). The Pearson correlation coefficient (CC) is given at the top of each panel. The environmental parameters in (a), (b) and (c) have an inverted y-axis to aid the visual comparison of the curves.

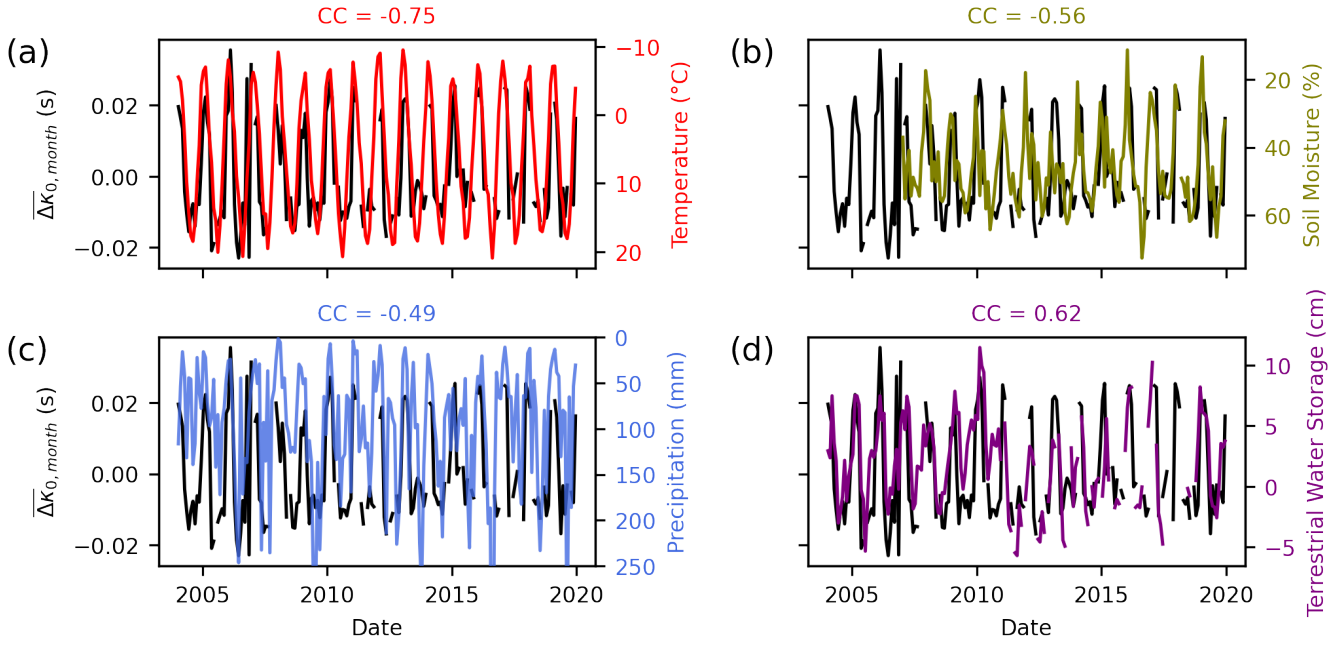

Figure 5 Same as Fig. 4 but for the cluster of sites in northeast Hokkaido (red triangles in Fig. 1).

highest at the beginning of January and gradually decreases until it reaches its lowest value in mid-August, after which $\Delta\kappa_0$ starts to increase again. We add to the plot the mean daily temperature averaged over the years 2004–2020. As already shown in Fig. 4(a), $\Delta\kappa_0$ is anti-correlated with temperature and has its minimum when the temperature is at its maximum. This is not consistent with Berger (1975), who provide a solution for thermoelastic strain in a homogeneous elastic halfspace due to surface temperature variations. According to this solution, the thermoelastic strain, and thus the velocity or attenuation changes at depth, should lag behind the surface temperature field by an order of magnitude depending on the wave period. For example, Richter et al. (2014) and Hillers et al. (2015) observe a time lag of 30 and 20 days, respectively, between annual air temperature and velocity variations. We do not observe such a delay between $\Delta\kappa_0$ and air temperature.

There are only few studies of seasonal shear wave velocity variations on Honshu. Wang et al. (2017) studied

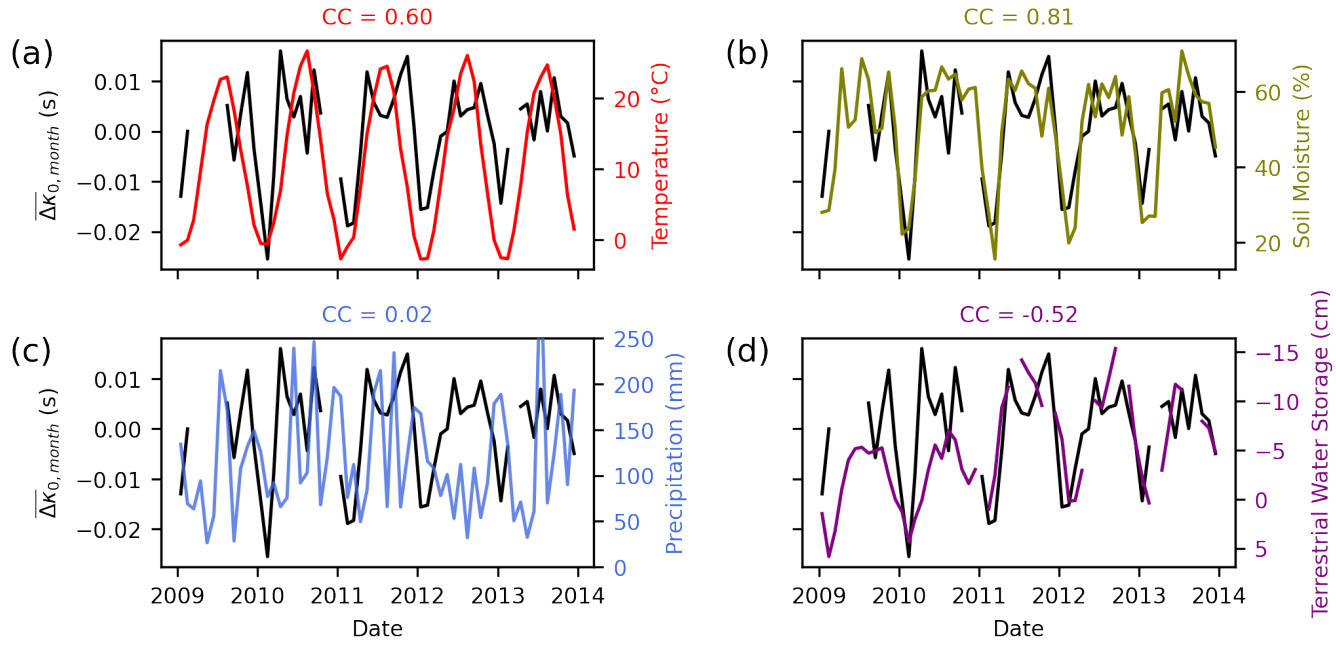

Figure 6 Same as Fig. 4 but for site YMTH07 (green triangle in Fig. 1) and only for the period 2009–2014. As opposed to Figures 4 and 5, the y-axis in (a), (b) and (c) is normal, whereas the y-axis in (d) is inverted.

noise-based seismic velocity changes throughout Japan using the Hi-net network. They do not observe seasonal velocity variations on the eastern side of Honshu, where our stations are located and where we observe strong seasonal effects of $\Delta\kappa_0$. However, Wang et al. (2017) measure in the 0.15–0.9 Hz frequency band and thus sample the crust to a depth of 8 km, which is much deeper than the KiK-net boreholes that we study (100–330 m). Miao et al. (2018) observe abrupt changes in seismic velocities at several KiK-net stations (four of which also show seasonal variations of $\Delta\kappa_0$: IBRH14, IWTH21, MYGH04, YMTH07) after high-intensity rainfall. Miao et al. (2018) use deconvolution interferometry between the 100-200 m deep borehole sensors and the surface sensor to compute the seismic velocities, but they relate the observed velocity changes to the water saturation of the uppermost sediments (first 1 m). In Fig. 4(b,c) we have a negative correlation of $\Delta\kappa_0$ with precipitation (CC=-0.43) and soil moisture (CC=-0.51). However, we observe gradual seasonal changes in $\Delta\kappa_0$, rather than abrupt changes that correlate with strong precipitation events.

The good correlation with TWS from GRACE/GRACE-FO satellite data (CC=0.60 in Fig. 4d) could also speak for a deeper origin of the $\Delta\kappa_0$ variations. The term 'deep' refers to a depth below the surface soil moisture where groundwater changes are relevant. Although precipitation is higher in summer, TWS has its minimum in summer, probably related to the fact that evapotranspiration rates exceed precipitation in summer, leading to a reduction of the total water volume in the ground. The good correlation between TWS and $\Delta\kappa_0$ is not present in the 2–3 years after the 2011 Tohoku earthquake. TWS values decrease after the earthquake, but there is no similar decrease in $\Delta\kappa_0$. This is because TWS is sensitive to earthquake-induced gravity changes on a larger regional scale, while $\Delta\kappa_0$ is a local parameter of the first hundred meters below a site. Because TWS data are derived from satellite data, the spatial resolution (300 km) and temporal resolution (1 month) are limited. Higher resolution data or direct measurements of groundwater levels would be needed to draw a definitive conclusion. Given the available data, we believe that groundwater fluctuations and the terrestrial water storage in the soil is the most likely explanation for the $\Delta\kappa_0$ variations at the Honshu sites.

5.3 Hokkaido site cluster: Correlation with frost and snow periods

Similar to Fig. 8, we stack all $\Delta\kappa_0$ values of the Hokkaido site cluster observed in the period 2004–2020 into one year and compute a smoothed curve using a Gaussian filter with a width of 6 days (Fig. 9). $\Delta\kappa_0$ is almost constant from May to November, but then increases quite rapidly until early January. In January and February, $\Delta\kappa_0$ is again almost constant, before returning to its original value between March and April.

Strong seasonal variations of seismic velocities in the northeastern corner of Hokkaido are also observed by Wang et al. (2017) using noise-based monitoring and by Miao et al. (2019) using earthquake seismic interferometry between surface and borehole stations of eight KiK-net sites. Both studies report an increase in seismic velocities in winter and almost constant velocities during the rest of the year, but have different explanations for the causes. Wang et al. (2017) reconstruct the observations using a linear relationship between the seismic velocity changes and the combined effects of pore pressure and snow depth. They argue that summer precipitation increases the pore pressure, while winter snow cover inhibits infiltration and groundwater recharge, resulting in lower pore pressure. Miao et al. (2019), on

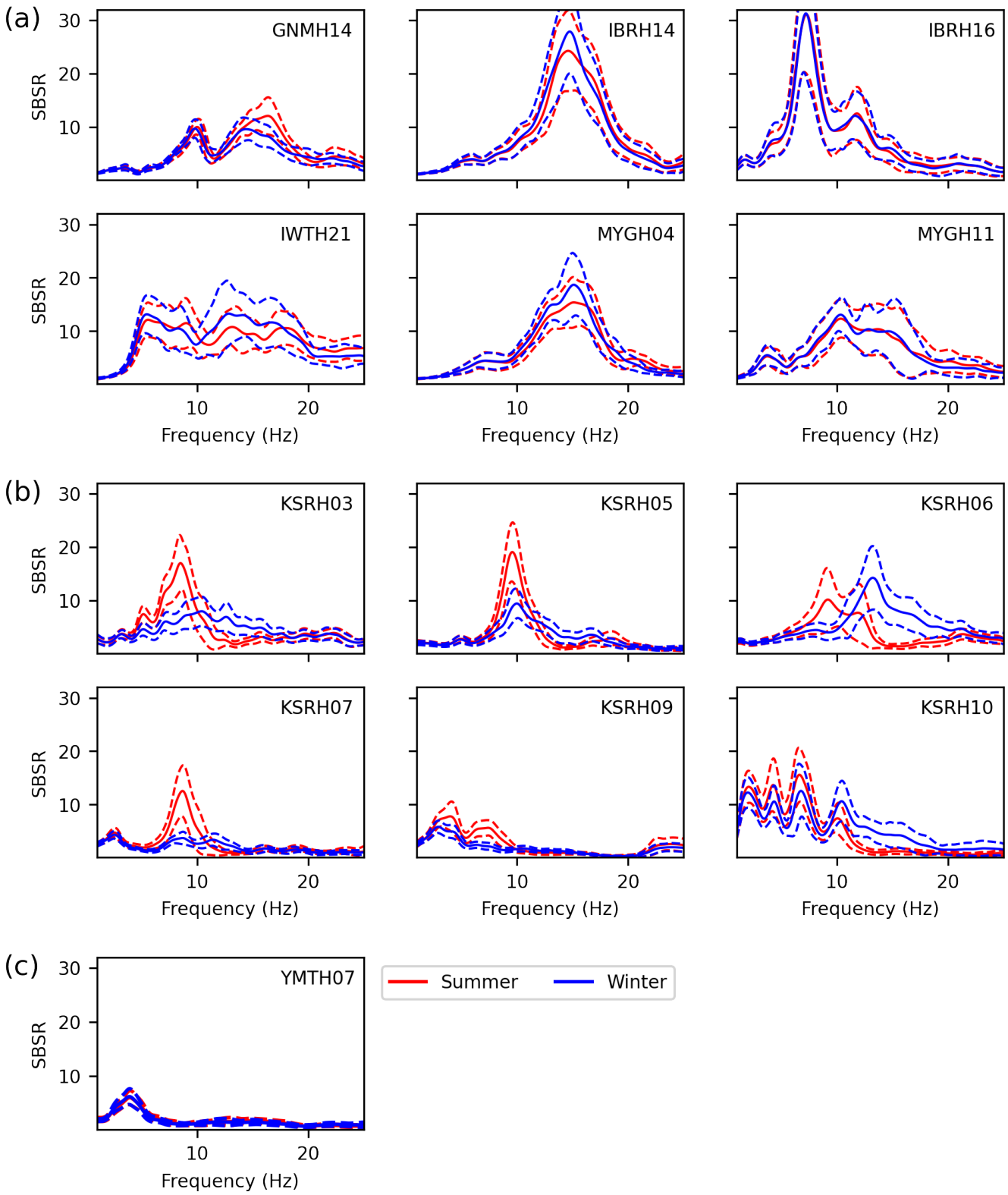

Figure 7 Surface-to-borehole spectral ratio (SBSR) computed for (a) stations on Honshu, (b) stations on Hokkaido, and (c) station YMTH07. Shown are the mean (solid line) and standard deviation (dashed lines) of the SBSRs obtained in summmer (red) and winter (blue). As summer months we used for (a) August, for (b) June-September, and for (c) July-September. As winter months we used for (a) January, for (b) January and February, and for (c) December-February.

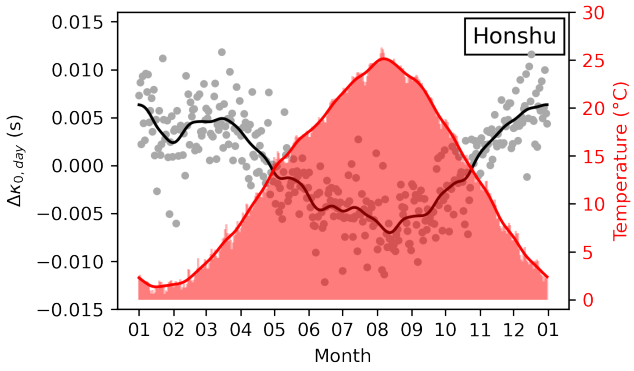

Figure 8 Stack of all 4626 $\Delta\kappa_0$ values observed in the period 2004–2020 in one year for the Honshu site cluster (blue triangles in Fig. 1). Gray dots: Mean $\Delta\kappa_0$ values for each day of the year and for each of the Honshu sites. Black curve: Mean curve computed from all gray dots, smoothed with a Gaussian filter of 6 days width. Red: Daily mean temperature stacked to one year (red bars) and smoothed a Gaussian filter of 6 days width (red curve).

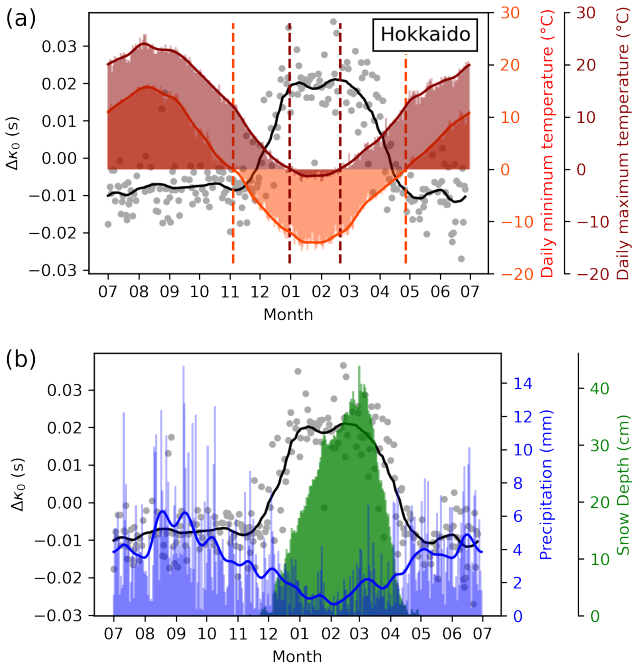

Figure 9 Stack of all 1331 $\Delta\kappa_0$ values observed in the period 2004–2020 into one year for the Hokkaido site cluster (red triangles in Fig. 1). The data is plotted from July to July to have the winter month in the middle. Gray dots: Mean $\Delta\kappa_0$ values for each day of the year and for each of the Hokkaido sites. Black curve: Mean curve computed from all gray dots, smoothed with a Gaussian filter of 6 days width. (a) Orange: Daily minimum temperature stacked to one year (bars) and smoothed with the same Gaussian filter (orange curve). Red: Same for the daily maximum temperature. The orange and red dashed lines mark the times where the minimum and maximum daily temperatures start to be below or above 0°C. (b) Blue: Total daily precipitation stacked to one year (bars) and smoothed using a Gaussian filter of 6 days width (blue curve). Green: Average depth of snow cover.

the other hand, associate the velocity changes in winter with the transition from unfrozen to frozen soil, where the main controlling factors are the cumulative and current temperature.

To better understand the driving mechanisms behind the $\Delta\kappa_0$ observations, we stack the daily minimum and maximum temperatures recorded on Hokkaido in the period 2004–2020 into one year and add this information to the plot in Fig. 9. While the changes in $\Delta\kappa_0$ occur quite rapidly and take only one and a half months, the temperature changes are more gradual so that thermoelastic strain is unlikely to be the cause for the variations in $\Delta\kappa_0$. However, there is a strong correlation with the times when the ground is frozen. $\Delta\kappa_0$ starts to increase in November which coincides with the time when the daily minimum temperature falls below 0°C (orange dashed line in Fig. 9) and the first frost occurs. $\Delta\kappa_0$ reaches its maximum when the daily maximum temperature is also below 0°C (red dashed line), at which point the ground is permanently frozen. $\Delta\kappa_0$ starts to decrease again when the daily maximum temperature exceeds 0°C in March and the ground thaws, and returns to its original value when the daily minimum temperature is also above 0°C. These observations seem to be consistent with Miao et al. (2019), who associate near-surface velocity changes with seasonally frozen soil. Similar observations have been obtained by Gassenmeier et al. (2014) and James et al. (2019), who report large velocity changes due to freezing and thawing processes in Brandenburg (Germany) and Alaska.

However, we doubt that a few centimeter-thick layer of frost could cause the broadband spectral changes in the SBSRs at frequencies as low as 5 Hz in Fig. 7(b). For example Kula et al. (2018) observe the signature of the 1.5–2 m deep permafrost layer on Svalbard at 35-45 Hz in the HVSR. Miao et al. (2019) report a frost depth of only 70 cm in northeastern Hokkaido and a shear-wave velocity increase up to a factor of 4–7 in this layer, depending on the soil. We therefore performed a simple test to see how a frozen surface layer can change the horizontal-to-surface spectral ratio (HVSR) at station KSRH03 and compare the results with real observations (see Table S3 and Figure S1 in the electronic supplementary material). A frozen layer with a thickness of 70 cm seems to be not sufficient to mimic the HVSR changes between summer and winter at KSRH03 and at frequencies below 20 Hz.

In contrast to Miao et al. (2019), Wang et al. (2017) argue that precipitation in summer and snowfall in winter drive the velocity changes on Hokkaido. To also explore this hypothesis, we plot the snow depth averaged over the period 2004–2020 in Fig. 9(b). The increase in $\Delta\kappa_0$ in November coincides with the start of the winter snow pack. $\Delta\kappa_0$ begins to decrease as the snow melts in spring. A Pearson's correlation coefficient of 0.73 is obtained between the mean curves of $\Delta\kappa_0$ and snow depth (Figure 10) that is comparable to the good correlation with temperature (Figure 5(a)). Snow load is unlikely to cause the changes in $\Delta\kappa_0$ because snow thickness increases throughout the winter, while kappa reaches a plateau value. According to Wang et al. (2017), the snow cover in winter inhibits the infiltration of water into the

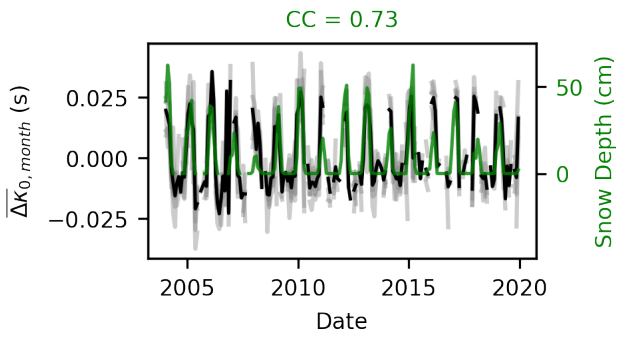

Figure 10 Monthly mean curve of $\Delta\kappa_0$ computed from all Hokkaido sites (red triangles in Fig. 1). Comparison with monthly mean snow depth.

ground. The frozen ground itself could act as a barrier for fluid flow to larger depths, which would explain the good correlation with minimum and maximum temperature. However, groundwater level in a well just 5 km away from site KSRH06 and at a similar elevation shows two annual maxima (Figure 4 in Yamaguchi et al., 2023). One peak is associated with spring snowmelt, and another smaller peak in the fall may be associated with precipitation after peak evapotranspiration in the summer and before the onset of frozen ground. We do not observe such a pattern with two maxima (or minima) for $\Delta\kappa_0$, but only an increased value of $\Delta\kappa_0$ in winter. Unlike the Honshu site cluster, TWS data do not provide a picture of soil water content and groundwater levels. This is because TWS data include the water contained in the surface snowpack. This snowpack water must be subtracted to obtain an estimate of the water in the ground. This is a difficult task because the snow water equivalent (the amount of water available in the snow) depends on e.g. temperature and changes over time.

Given the above observations and data, we cannot identify the main cause for the observed increase of $\Delta\kappa_0$ in winter. The mean curve of $\Delta\kappa_0$ shows good correlation with periods of frozen ground, but also with snow pack that inhibits water infiltration. It is difficult to separate the influences of different environmental parameters because they are often interrelated. For example, the presence snow pack in winter also correlates with the times when the air temperature is below zero. Local groundwater data and systematic modeling of a surface frost layer could help to understand the $\Delta\kappa_0$ variations.

5.4 Site YMTH07

Site YMTH07 is the only site where $\Delta\kappa_0$ is higher in summer than winter, which is the opposite of what we observed at all other sites with seasonal trends. In Fig. 11, we stack all $\Delta\kappa_0$ values at site YMTH07 observed in the period 2009–2014 into one year and compute a smoothed curve. The mean $\Delta\kappa_0$ curve has a similar box shape as the mean $\Delta\kappa_0$ curve on Hokkaido, only with the opposite sign (Fig. 11), suggesting a similar cause related to frost and snow. Mean temperatures at YMTH07 are not as negative in winter as on Hokkaido (-2°C at YMTH07 and -10°C on Hokkaido, see Figures

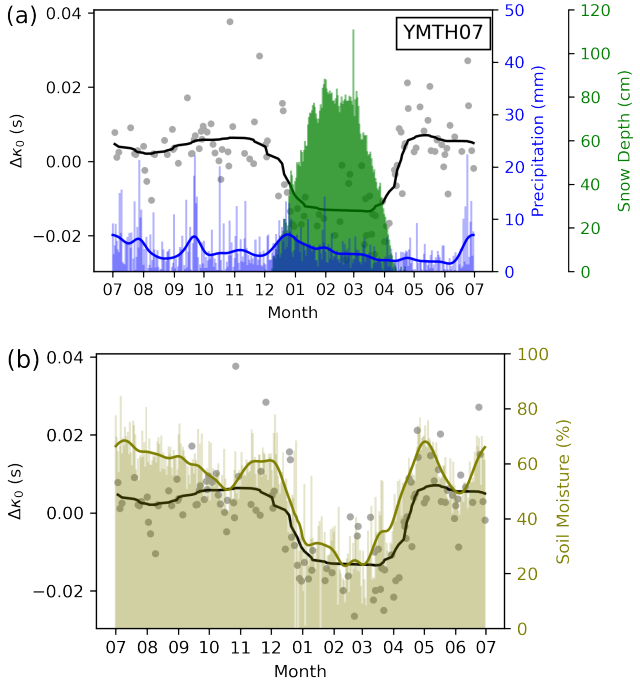

Figure 11 Stack of all 145 $\Delta\kappa_0$ values observed in the period 2009–2014 at YMTH07 (green triangle in Fig. 1) into one year. Gray dots: Mean $\Delta\kappa_0$ values for each day of the year. Black curve: Mean curve computed from all gray dots, smoothed with a Gaussian filter of 6 days width. (a) Blue curve: Total daily precipitation stacked to one year (bars) and smoothed with the same Gaussian filter (blue curve). Green: Average depth of snow cover. (b) Olive curve: Same as for (a) but for daily soil moisture content.

6(a) and 5(a), respectively), but snow depth is greater (winter snow depth up to 100 cm at YMTH07 and 50 cm on Hokkaido, see Figures 12 and 10, respectively). In Fig. 11(a), we therefore add snow depth and precipitation to the plot. The formation of a permanent snow pack in the fall and the end of the snow season in spring coincide with the times when $\Delta\kappa_0$ begins to decrease in fall or returns to its original value in spring, respectively. The maximum snow depth is reached in February, before it begins to melt in March. If we plot monthly mean snow depth and $\Delta\kappa_0$ variations over time (Figure 12), we obtain a Pearson's correlation coefficient of CC=-0.71.

In Figures 6(b) and 11, we observe a very good correlation of $\Delta\kappa_0$ with soil moisture content. The correlation coefficient between $\Delta\kappa_0$ and soil moisture is CC=0.81 and the mean soil moisture curve in Figure 6(b) has a similar shape as $\Delta\kappa_0$. It is unlikely that $\Delta\kappa_0$ reacts to soil moisture changes within the upper few centimeters. But soil moisture content is influenced by snow cover and frozen soil, which limit water infiltration.

One explanation for the opposite sign at YMTH07 compared to all other sites could be that at site YMTH07 site amplification is negligible and the differences in SBSR between summer and winter are very small. The choice of the frequency window for $\Delta\kappa_0$ estimation then could have a large impact on whether or not the value of $\Delta\kappa_0$ will be positive in winter. We therefore

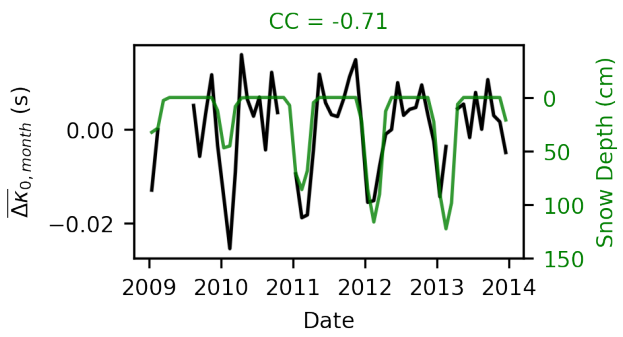

Figure 12 Monthly mean curve of $\Delta\kappa_0$ (black curve) computed at YMTH07 (green triangle in Fig. 1). Comparison with monthly snow depth (green).

lowered the frequency band from 12-24 Hz to 10-22 Hz and to 8-20 Hz for the computation of $\Delta\kappa_0$. The sign of the seasonal variations of $\Delta\kappa_0$ does not change but the magnitude of the seasonality becomes less pronounced. While all other sites are in alluvial valleys with similar surface elevations to nearby rivers, YMTH07 is located on a fluvial terrace 40 m above the nearest river. Its higher elevation on a high permeability terrace could result in a significantly lower water table compared to the other sites. This could have unrecognized effects on amplification and the resulting seasonality of $\Delta\kappa_0$.

5.5 Application in other regions of the world and implications for ground motion prediction and seismic hazard analysis

The dense station coverage and availability of co-located borehole and surface sensors in Japan provide a unique opportunity to study $\Delta\kappa_0$. Such data availability is rare in other parts of the world. In regions without borehole sensors, an alternative is to calculate κ at a surface station for individual events and use a traditional distance regression (Eq. 2) to estimate the path term. By subtracting the path term from individual κ values, κ_0 at the surface can be estimated as a function of time. While this approach cannot remove possible influences from the seismic source, it could still allow for the detection of seasonal variability in surface κ_0 comparable to $\Delta\kappa_0$. In regions with sparse ground motion data, the detection of seasonal variations in κ_0 or $\Delta\kappa_0$ becomes even more challenging. However, our study shows a relationship between $\Delta\kappa_0$ variations and changes in the SBSR and HVSR. This relationship suggests that alternative techniques, such as HVSR calculated from ambient noise recordings, could be used to assess seasonal variations in site response. Although HVSR does not provide direct measurements of κ_0, it could serve as an indicator of whether κ_0 might be affected by seasonal effects.

The parameter κ_0 was originally defined as a measure of the time-independent high-frequency attenuation at a site. Our study shows that, contrary to its original definition, $\Delta\kappa_0$ can be significantly influenced by seasonal broadband changes in the seismic site response (Fig. 7). The parameter is highly sensitive to even small frequency and amplitude variations, as observed for example at the Honshu site cluster and station YMTH07. There, the observed SBSR changes between summer and winter are relatively small, but $\Delta\kappa_0$ effectively captures these subtle variations. In contrast, the Hokkaido sites show more pronounced changes in SBSR between seasons, with strong amplification differences over a wide frequency range. These changes in SBSR suggest time-dependent variations in the characteristics of the ground shaking in terms of the predicted intensity, duration and frequency content.

The seasonal variation of κ_0 contributes to a better understanding of high-frequency ground motions. Indeed, the recent development of Fourier domain ground motion prediction models has highlighted the high variability of high-frequency seismic ground motions (Stafford, 2017; Bayless and Abrahamson, 2018; Bora et al., 2019). Both site-to-site and within-station variability increase at high frequencies. Above 10 Hz, site-specific attenuation models are unable to explain the observed site-to-site variability (Pilz et al., 2025). Our study provides a physical explanation for the increase in within-station variability, which may be partly due to seasonal variations. As seasonal variations are highly station dependent, they may also explain the site-to-site ground motion variability.

These seasonal variations in ground motions may have implications for Probabilistic Seismic Hazard Analysis (PSHA). Indeed, a key assumption of a standard PSHA model is that earthquake occurence and ground motions can be modeled as a time-independent Poisson process. PSHA models consist of two main components: a source model that predicts the frequency and location of future earthquakes, and a ground-motion prediction model. Many studies have proposed the replacement of Poisson time-independent seismicity models with time-dependent seismicity models and the transition to time-dependent seismic hazard models (e.g. Akinci et al., 2009; Boyd, 2012; Chang et al., 2017). Our study also suggests a possible temporal dependence of ground motions which, to our knowledge, has never been considered in a PSHA framework. Incorporating this temporal variation of ground motions into seismic hazard calculations will be difficult, as these variations appear to be highly site-dependent. Therefore, only non-ergodic (site-specific) ground motion prediction models (and corresponding site-specific seismic hazard models) could take these variations into account. In site specific seismic hazard models, κ_0 is mainly used to adjust Ground-motion Prediction Equations (GMPEs) or a backbone GMPE to the target site. This is usually done within a logic tree framework. One way to account for seasonal variations in κ_0 would then be to have different branches of the logic tree for different seasons. Such additional branches should be accompanied by a reduction in the aleatory variability of κ_0 and associated ground motion models. Such a reduction will require specific research.

6 Conclusion

In this study, we have computed $\Delta\kappa_0$ (κ_0 between a borehole and a surface station) at 188 KiK-net sites. The

value of $\Delta\kappa_0$ that we provide is, in contrast to its original definition by Anderson and Hough (1984), an integrative parameter of site amplification and effective attenuation (intrinsic and scattering attenuation). We observe clear seasonal variations at 13 KiK-net sites located in northeastern Hokkaido and on Honshu, where $\Delta\kappa_0$ is generally larger in winter than in summer on the order of tens of milliseconds. While temporal velocity variations have already been observed in the past, this is the first time this has been done for the high frequency spectral shape. The parameter κ is a very sensitive measure for detecting seasonal variations in high frequency site effects because it is a measure of slope. In contrast, changes in the predominant frequency of amplification can only be detected if the change is greater than the sampling frequency of the time series. A slope difference such as $\Delta\kappa_0$, on the other hand, can detect smaller changes.

There are three main clusters of sites in Japan that respond differently to environmental forcing. On the eastern side of Honshu, $\Delta\kappa_0$ changes are more gradual and are likely to respond to the water content at depth, as shown by the good correlation with TWS. In northeastern Hokkaido, $\Delta\kappa_0$ values are well correlated with frost times and a permanent snow cover in winter. However, it is unclear whether the frozen surface layer or water changes in the subsurface cause the changes in $\Delta\kappa_0$. At site YMTH07, $\Delta\kappa_0$ behaves opposite to all other sites, but correlates well with soil moisture and snow depth. These are preliminary interpretations and further, more localised studies are needed to fully understand the driving mechanisms behind the changes in $\Delta\kappa_0$ in each region.

Climate change affects seismic hazard through changes in seismicity as has been shown for example by Bohnhoff et al. (2024). In this study, we show that another component, the high-frequency shaking, should also be considered. For example, on Hokkaido, the whole spectrum changes over a wide range of frequencies. The amplitude of the surface-to-borehole spectral ratio in winter is sometimes reduced by a factor of two compared to summer, which affects the level of shaking at these sites. Local site conditions respond to environmental changes such as temperature, snow depth, soil moisture and groundwater content. Rising global mean temperatures will potentially change local environmental parameters (e.g. groundwater level, number of frost days, frequency of floods) which will then affect the site response and the shaking at a site. Currently, such processes are not considered in seismic hazard analysis. The sensitivity of near-surface parameters to environmental forcing provides also an opportunity to use seismology as a tool to monitoring climate change. For example, Clements and Denolle (2023) found a long-term trend in seismic velocities in California that they associate with the lowering of the groundwater table in the area. The future development and deployment of multi-parameter stations that monitor both ground motion and environmental parameters (temperature, precipitation, soil moisture, groundwater level) will be required for this type of studies.

Researchers generally focus on seismic velocity changes, but $\Delta\kappa_0$ may also serve as an effective parameter for detecting seasonal variations in site effects, particularly at high frequencies. More research and additional data are needed to understand the driving mechanisms behind the observed $\Delta\kappa_0$ variations of this study, and also why we observe strong seasonal variations at some stations but not at other nearby stations. For example, local groundwater data could help to improve our understanding of fluid processes at depth. New technologies, such as distributed acoustic sensing (DAS) using fibre optic cables could provide data with high spatiotemporal resolution to study near-surface seasonal variations (Shen, 2022). More research is also needed to assess how systematic these changes in the high-frequency site response are and to evaluate their potential impact on current seismic hazard analysis practices.

Acknowledgements

We are very grateful for the feedback and suggestions of two anonymous reviewers, which helped to improve our manuscript. We would also like to thank the National Research Institute for Earth Science and Disaster Resilience (NIED) for providing the KiK-net data, and the JMA Japan Meteorological Agency and the Copernicus Climate Change Service (C3S) for weather and soil moisture data. Eva Boergens helped us to access and process the GRACE satellite data. We thank Miyamoto Hitoshi and Oishi Tetsuya from Shibaura Institute of Technology, and Inagaki Daigo, Gotou Yuji, and Sagai Kiyotaka from MLIT for their help accessing groundwater datasets. This work has also benefited from support of the European Union's Horizon Europe research and innovation programme project COREu (grant agreement No. 101136217).

Data and code availability

Kik-net data for this study (seismograms, metadata and v_s profiles) are downloaded from the website https://www.kyoshin.bosai.go.jp/ (last accessed January 2022) and are provided by the National Research Institute for Earth Science and Disaster Resilience (NIED, 2019). Daily weather data are downloaded from the JMA Japan Meteorological Agency (https://www.data.jma.go.jp/gmd/risk/obsdl/index.php, last accessed July 2024). Soil moisture gridded data are provided by the Copernicus Climate Change Service, Climate Data Store (Dorigo et al., 2019, last accessed June 2024). Terrestrial Water Storage (TWS) variability data for Japan are extracted from the Gravity Recovery And Climate Experiment (GRACE) and GRACE Follow-on (GRACE-FO) Level-3 products COST-G RL01 (Boergens et al., 2020, last accessed June 2024). We used Python and ObsPy, a Python framework for seismology (Beyreuther et al., 2010), to analyze the data and to generate the figures. The maps were plotted using the Generic Mapping Tools (GMT) version 5.4.3 (www.soest.hawaii.edu/gmt, last accessed March 2019; Wessel and Smith, 1998).

Competing interests

The authors have no competing interests.

References

Akinci, A., Galadini, F., Pantosti, D., Petersen, M., Malagnini, L., and Perkins, D. Effect of time dependence on probabilistic seismic-hazard maps and deaggregation for the Central Apennines, Italy. *Bulletin of the Seismological Society of America*, 99 (2A):585–610, 2009. doi: https://doi.org/10.1785/0120080053.

Anderson, J. G. and Hough, S. E. A model for the shape of the Fourier amplitude spectrum of acceleration at high frequencies. *Bull. Seismol. Soc. Am.*, 74(5):1969–1993, 1984. doi: https://doi.org/10.1785/BSSA0740051969.

Aoi, S., Kunugi, T., and Fujiwara, H. Strong-motion seismograph network operated by NIED: K-NET and KiK-net. *Journal of Japan Association for Earthquake Engineering*, 4(3):65–74, 2004. doi: https://doi.org/10.5610/jaee.4.3_65.

Bayless, J. and Abrahamson, N. An empirical model for Fourier amplitude spectra using the NGA-West2 database. PEER Report 2018/07, Pacific Earthquake Engineering Research Center, University of California, Berkeley, California, 2018.

Beresnev, I. A. Interpretation of kappa and fmax filters as source effect. *Bull. Seismol. Soc. Am.*, 109(2):822–826, 2019. doi: https://doi.org/10.1785/0120180250.

Berger, J. A note on thermoelastic strains and tilts. *Journal of Geophysical Research*, 80(2):274–277, 1975. doi: https://doi.org/10.1029/JB080i002p00274.

Beyreuther, M., Barsch, R., Krischer, L., Megies, T., Behr, Y., and Wassermann, J. ObsPy: A Python toolbox for seismology. *Seismol. Res. Lett.*, 81(3):530–533, 2010. doi: 10.1785/gssrl.81.3.530.

Bindi, D., Picozzi, M., Spallarossa, D., Cotton, F., and Kotha, S. R. Impact of magnitude selection on aleatory variability associated with ground-motion prediction equations: Part II—analysis of the between-event distribution in central Italy. *Bull. Seismol. Soc. Am.*, 109(1):251–262, 2019. doi: https://doi.org/10.1785/0120180239.

Boergens, E., Dobslaw, H., and Dill, R. COST-G GravIS RL01 Continental Water Storage Anomalies. V. 0005. GFZ Data Services, https://doi.org/10.5880/COST-G.GRAVIS_01_L3_TWS, 2020.

Bohnhoff, M., Martínez-Garzón, P., and Ben-Zion, Y. Global Warming Will Increase Earthquake Hazards through Rising Sea Levels and Cascading Effects. *Seismol. Res. Lett.*, page Early Publication, 2024. doi: https://doi.org/10.1785/0220240100.

Bora, S. S., Cotton, F., Scherbaum, F., Edwards, B., and Traversa, P. Stochastic source, path and site attenuation parameters and associated variabilities for shallow crustal European earthquakes. *Bull. Earthquake Eng.*, 15(11):4531–4561, 2017. doi: https://doi.org/10.1007/s10518-017-0167-x.

Bora, S. S., Cotton, F., and Scherbaum, F. NGA-West2 empirical Fourier and duration models to generate adjustable response spectra. *Earthquake Spectra*, 35(1):61–93, 2019. doi: https://doi.org/10.1193/110317EQS228M.

Boyd, O. S. Including foreshocks and aftershocks in time-independent probabilistic seismic-hazard analyses. *Bulletin of the Seismological Society of America*, 102(3):909–917, 2012. doi: https://doi.org/10.1785/0120110008.

Chang, Y.-W., Loh, C.-H., and Jean, W.-Y. Time-predictable model application in probabilistic seismic hazard analysis of faults in Taiwan. *Terrestrial, Atmospheric & Oceanic Sciences*, 28(6), 2017. doi: https://doi.org/10.3319/TAO.2017.02.08.01.

Clements, T. and Denolle, M. The seismic signature of California's earthquakes, droughts, and floods. *Journal of Geophysical Research: Solid Earth*, 128(1):e2022JB025553, 2023. doi: https://doi.org/10.1029/2022JB025553.

Colombero, C., Baillet, L., Comina, C., Jongmans, D., Larose, E., Valentin, J., and Vinciguerra, S. Integration of ambient seismic noise monitoring, displacement and meteorological measurements to infer the temperature-controlled long-term evolution of a complex prone-to-fall cliff. *Geophysical Journal International*, 213(3):1876–1897, 2018. doi: https://doi.org/10.1093/gji/ggy090.

Dorigo, W., Preimesberger, W., Reimer, C., Van der Schalie, R., Pasik, A., De Jeu, R., and Paulik, C. Soil moisture gridded data from 1978 to present, v202212, 2019. doi: https://doi.org/10.24381/cds.d7782f18.

Edwards, B., Ktenidou, O.-J., Cotton, F., Abrahamson, N., Van Houtte, C., and Fäh, D. Epistemic uncertainty and limitations of the κ_0 model for near-surface attenuation at hard rock sites. *Geophys. J. Int.*, 202(3):1627–1645, 2015. doi: https://doi.org/10.1093/gji/ggv222.

Gassenmeier, M., Sens-Schönfelder, C., Delatre, M., and Korn, M. Monitoring of environmental influences on seismic velocity at the geological storage site for CO2 in Ketzin (Germany) with ambient seismic noise. *Geophysical Journal International*, 200(1): 524–533, 2014. doi: https://doi.org/10.1093/gji/ggu413.

Haendel, A., Anderson, J. G., Pilz, M., and Cotton, F. A frequency-dependent model for the shape of the Fourier amplitude spectrum of acceleration at high frequencies. *Bull. Seismol. Soc. Am.*, 110(6):2743–2754, 2020. doi: https://doi.org/10.1785/0120200118.

Haendel, A., Pilz, M., and Cotton, F. Temporal variations of $\Delta\kappa_0$. In Arion, C., Scupin, A., and Ţigănescu, A., editors, *Proceedings of the 3rd European Conference on Earthquake Engineering and Seismology (ECEES): September 4-9, 2022, Bucharest, Romania*, pages 4937–4943, 2022.

Haendel, A., Pilz, M., and Cotton, F. Hard-Rock κ_0 at KiK-Net Sites in Japan. *Bulletin of the Seismological Society of America*, 113 (6):2650–2665, 2023. doi: https://doi.org/10.1785/0120220246.

Hillers, G., Campillo, M., and Ma, K.-F. Seismic velocity variations at TCDP are controlled by MJO driven precipitation pattern and high fluid discharge properties. *Earth and Planetary Science Letters*, 391:121–127, 2014. doi: https://doi.org/10.1016/j.epsl.2014.01.040.

Hillers, G., Ben-Zion, Y., Campillo, M., and Zigone, D. Seasonal variations of seismic velocities in the San Jacinto fault area observed with ambient seismic noise. *Geophysical Journal International*, 202(2):920–932, 2015. doi: https://doi.org/10.1093/gji/ggv151.

Hollender, F., Roumelioti, Z., Maufroy, E., Traversa, P., and Mariscal, A. Can we trust high-frequency content in strong-motion database signals? Impact of housing, coupling, and installation depth of seismic sensors. *Seismol. Res. Lett.*, 91(4):2192–2205, 2020. doi: https://doi.org/10.1785/0220190163.

Illien, L., Andermann, C., Sens-Schönfelder, C., Cook, K., Baidya, K., Adhikari, L., and Hovius, N. Subsurface moisture regulates Himalayan groundwater storage and discharge. *AGU Advances*, 2(2):e2021AV000398, 2021. doi: https://doi.org/10.1029/2021AV000398.

James, S., Knox, H., Abbott, R., Panning, M., and Screaton, E. Insights into permafrost and seasonal active-layer dynamics from ambient seismic noise monitoring. *Journal of Geophysical Research: Earth Surface*, 124(7):1798–1816, 2019. doi: https://doi.org/10.1029/2019JF005051.

Ji, C., Cabas, A., Cotton, F., Pilz, M., and Bindi, D. Within-station variability in kappa: Evidence of directionality effects.

Bull. Seismol. Soc. Am., 110(3):1247–1259, 2020. doi: https://doi.org/10.1785/0120190253.

Ji, C., Cabas, A., Bonilla, L. F., and Gelis, C. Effects of nonlinear soil behavior on Kappa (κ): Observations from the KiK-Net database. *Bull. Seismol. Soc. Am.*, 111(4):2138–2157, 2021. doi: https://doi.org/10.1785/0120200286.

Kilb, D., Biasi, G., Anderson, J., Brune, J., Peng, Z., and Vernon, F. L. A comparison of spectral parameter kappa from small and moderate earthquakes using southern California ANZA seismic network data. *Bull. Seismol. Soc. Am.*, 102(1):284–300, 2012. doi: https://doi.org/10.1785/0120100309.

Köhler, A. and Weidle, C. Potentials and pitfalls of permafrost active layer monitoring using the HVSR method: A case study in Svalbard. *Earth Surface Dynamics*, 7(1):1–16, 2019. doi: https://doi.org/10.5194/esurf-7-1-2019.

Ktenidou, O.-J., Gélis, C., and Bonilla, L.-F. A study on the variability of kappa (κ) in a borehole: Implications of the computation process. *Bull. Seismol. Soc. Am.*, 103(2A):1048–1068, 2013. doi: https://doi.org/10.1785/0120120093.

Kula, D., Olszewska, D., Dobiński, W., and Glazer, M. Horizontal-to-vertical spectral ratio variability in the presence of permafrost. *Geophysical Journal International*, 214(1):219–231, 2018. doi: https://doi.org/10.1093/gji/ggy118.

Li, G. and Ben-Zion, Y. Daily and seasonal variations of shallow seismic velocities in southern California from joint analysis of H/V ratios and autocorrelations of seismic waveforms. *Journal of Geophysical Research: Solid Earth*, 128(2):e2022JB025682, 2023. doi: https://doi.org/10.1029/2022JB025682.

Lotti, A., Pazzi, V., Saccorotti, G., Fiaschi, A., Matassoni, L., Gigli, G., et al. HVSR analysis of rockslide seismic signals to assess the subsoil conditions and the site seismic response. *International Journal of Geophysics*, 2018, 2018. doi: https://doi.org/10.1155/2018/9383189.

Malagnini, L., Dreger, D. S., Bürgmann, R., Munafò, I., and Sebastiani, G. Modulation of seismic attenuation at Parkfield, before and after the 2004 M6 earthquake. *Journal of Geophysical Research: Solid Earth*, 124(6):5836–5853, 2019. doi: https://doi.org/10.1029/2019JB017372.

Mao, S., Lecointre, A., van der Hilst, R. D., and Campillo, M. Space-time monitoring of groundwater fluctuations with passive seismic interferometry. *Nature Communications*, 13(1):4643, 2022. doi: https://doi.org/10.1038/s41467-022-32194-3.

Mayor, J., Bora, S. S., and Cotton, F. Capturing regional variations of hard-rock κ_0 from coda analysis. *Bull. Seismol. Soc. Am.*, 108 (1):399–408, 2018. doi: https://doi.org/10.1785/0120170153.

Miao, Y., Shi, Y., and Wang, S.-Y. Temporal change of near-surface shear wave velocity associated with rainfall in Northeast Honshu, Japan. *Earth, Planets and Space*, 70:1–11, 2018. doi: https://doi.org/10.1186/s40623-018-0969-3.

Miao, Y., Shi, Y., Zhuang, H., Wang, S., Liu, H., and Yu, X. Influence of seasonal frozen soil on near-surface shear wave velocity in eastern Hokkaido, Japan. *Geophysical Research Letters*, 46(16): 9497–9508, 2019. doi: https://doi.org/10.1029/2019GL082282.

Nakamura, Y. A method for dynamic characteristics estimation of subsurface using microtremor on the ground surface. *Railway Technical Research Institute, Quarterly Reports*, 30(1), 1989.

NIED. NIED K-NET, KiK-net, National Research Institute for Earth Science and Disaster Resilience. doi:10.17598/NIED.0004, 2019.

Papageorgiou, A. S. and Aki, K. A specific barrier model for the quantitative description of inhomogeneous faulting and the prediction of strong ground motion. Part II. Applications of the model. *Bull. Seismol. Soc. Am.*, 73(4):953–978, 1983. doi: https://doi.org/10.1785/BSSA0730040953.

Perron, V., Laurendeau, A., Hollender, F., Bard, P.-Y., Gélis, C., Traversa, P., and Drouet, S. Selecting time windows of seismic phases and noise for engineering seismology applications: A versatile methodology and algorithm. *Bull. Earthq. Eng.*, 16 (6):2211–2225, 2018. doi: https://doi.org/10.1007/s10518-017-0131-9.

Pilz, M., Cotton, F., and Zhu, C. Site-response high-frequency frontiers and the added value of site-specific earthquake record-based measurements of velocity and attenuation. *Earthquake Spectra*, 2025. doi: https://doi.org/10.1177/87552930241311312.

Richter, T., Sens-Schönfelder, C., Kind, R., and Asch, G. Comprehensive observation and modeling of earthquake and temperature-related seismic velocity changes in northern Chile with passive image interferometry. *Journal of Geophysical Research: Solid Earth*, 119(6):4747–4765, 2014. doi: https://doi.org/10.1002/2013JB010695.

Sens-Schönfelder, C. and Wegler, U. Passive image interferometry and seasonal variations of seismic velocities at Merapi Volcano, Indonesia. *Geophysical research letters*, 33(21), 2006. doi: https://doi.org/10.1029/2006GL027797.

Shen, Z. *Probing water below the surface: Insights from seismic interferometry with conventional and DAS array*. PhD Thesis, California Institute of Technology, Pasadena, California, 2022. doi: https://doi.org/10.7907/5vtn-1c34.

Stafford, P. J. Interfrequency correlations among Fourier spectral ordinates and implications for stochastic ground-motion simulation. *Bulletin of the Seismological Society of America*, 107(6): 2774–2791, 2017. doi: https://doi.org/10.1785/0120170081.

Tafreshi, M. D., Bora, S. S., Ghofrani, H., Mirzaei, N., and Kazemian, J. Region-and site-specific measurements of kappa (κ_0) and associated variabilities for Iran. *Bull. Seismol. Soc. Am.*, 112(6): 3046–3062, 2022. doi: https://doi.org/10.1785/0120210315.

Van Houtte, C., Ktenidou, O.-J., Larkin, T., and Holden, C. Hard-site κ_0 (kappa) calculations for Christchurch, New Zealand, and comparison with local ground-motion prediction models. *Bull. Seismol. Soc. Am.*, 104(4):1899–1913, 2014. doi: https://doi.org/10.1785/0120130271.

Vassallo, M., Cultrera, G., Di Giulio, G., Cara, F., and Milana, G. Peak frequency changes from HV spectral ratios in central Italy: Effects of strong motions and seasonality over 12 years of observations. *Journal of Geophysical Research: Solid Earth*, 127(5):e2021JB023848, 2022. doi: https://doi.org/10.1029/2021JB023848.

Wang, Q.-Y., Brenguier, F., Campillo, M., Lecointre, A., Takeda, T., and Aoki, Y. Seasonal crustal seismic velocity changes throughout Japan. *Journal of Geophysical Research: Solid Earth*, 122(10):7987–8002, 2017. doi: https://doi.org/10.1002/2017JB014307.

Wessel, P. and Smith, W. H. F. New, improved version of generic mapping tools released. *EOS, Trans. Am. Geophys. Un.*, 79(47): 579, 1998. doi: https://doi.org/10.1029/98EO00426.

Xu, B. and Rathje, E. M. The effect of soil nonlinearity on high-frequency spectral decay and implications for site response analysis. *Earthq. Spectra*, 37(2):686–706, 2021. doi: https://doi.org/10.1177/8755293020981991.

Yamaguchi, T., Miyamoto, H., and Oishi, T. Using Simple LSTM Models to Evaluate Effects of a River Restoration on Groundwater in Kushiro Wetland, Hokkaido, Japan. *Water*, 15(6):1115, 2023. doi: https://doi.org/10.3390/w15061115.